RSC Advances

ROYAL SOCIETY OF CHEMISTRY

www.rsc.org/advances

Graphical Abstract：

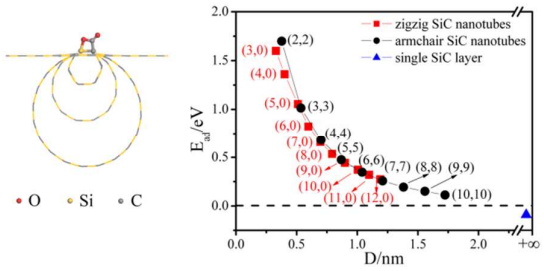

CO_2 adsorption and reduction on SiC nanomaterials display a curvature effect.

Curvature Effect of SiC Nanotubes and Sheet for CO_2 Capture and Reduction

P. Zhang[1,2], X. L. Hou[1,*], J. L. Mi[1], Q. Jiang,[3] H. Aslan[2], M. D. Dong[2,*]

[1] *Institute for Advanced Materials, and School of Materials Science and Engineering, Jiangsu University, Zhenjiang 212013, China.*

[2] *Center for DNA Nanotechnology (CDNA), interdisciplinary Nanoscience Center (iNANO), Aarhus University, DK-8000 Aarhus, Denmark.*

[3] *Key Laboratory of Automobile Materials, Ministry of Education, and Department of Materials Science and Engineering, Jilin University, Changchun 130022, China.*

Abstract

Environmental crisis due to greenhouse gas CO_2 emissions is motivating researchers to discover new materials and efficient technologies for CO_2 capture and conversion. In this work, the density functional theory (DFT) has been employed to investigate the surface curvature dependence of the adsorption and (electro) reduction of CO_2 on SiC nanomaterials, including single layer SiC sheets and nanotubes. The DFT calculations show that both the adsorption energy and reduction free energy decrease with the decrease of the curvature of SiC nanotubes. SiC nanotubes with suitable curvature can capture and reduce CO_2 effectively. However single layer SiC sheet (without curvature) cannot adsorb CO_2 at all. These findings are particularly relevant to generate fuels with a carbon-neutral footprint.

Keywords: Curvature effect, SiC nanomaterials, CO_2 capture, CO_2 reduction, Density functional theory

*Corresponding author. Email: houxiuli@ujs.edu.cn, dong@inano.au.dk

Introduction

The global climate change has become a significant challenge due to the magnitude of greenhouse gases emission. CO_2 is believed to be partly responsible due to the combustion of fossil fuels.[1,2] CO_2 chemistry has become a very attractive area of research, not only because of environmental concerns, but also due to the potential use of CO_2 as an alternative and economical feedstock.[3] The recovery of CO_2 for its hydrogenation to formic acid, alcohols or other hydrocarbon compounds is an important approach to recycle the released CO_2. However, it is a difficult task due to the challenges associated with the chemical inertness of CO_2.

The combination of CO_2 capture and conversion is an attractive strategy for efficiently reducing CO_2 emissions. One example of CO_2 conversion to a useful hydrocarbon is hydrogenation of CO_2 to formic acid, an important chemical fuel in fuel cells.[4,5] An ideal CO_2 sequestration material should have large surface area and strong adsorption ability. Several CO_2 adsorbents have been proposed previously including zeolite, carbon, boron nitride, alumina and metal-organic frameworks (MOFs).[6-16] Recently, it has been shown that CO_2 can be adsorbed strongly on boron antisite in boron-rich boron nitride (BN) nanotubes.[17] In addition, the process of CO_2 capture/release can be simply controlled by switching on/off the charges carried by BN nanomaterials.[18] A lot of attention has also been focused on the hydrogenation of CO_2 on metals, carbides, and metal/oxide catalysts.[19-30] Cu electrodes, of all experimentally examined metals, have shown a unique ability to produce hydrocarbon products at reasonable currents and efficiencies, but with a still relatively large

over-potential of approximately 1 V.[31,32] Carbon monoxide dehydrogenase (CODH) enzyme has been shown to have better catalytic activity than Cu.[25] With a Pt working electrode in acidic pyridine solutions, CO_2 can be reduced by H atoms bound to the Pt surface that are transferred to CO_2 in a proton-coupled hydride transfer mechanism activated by pyridinium at low over-potentials (–0.58 V vs SCE).[33,34] It is essential that the materials can capture and convert CO_2 at atmospheric pressure and room temperature with only heat from surrounding environments to avoid the generation of new CO_2.[8] Thus far, few materials can satisfy these requirements.[8]

SiC with the atomic ratio of 1:1 can be potentially provide a lot of active sites for CO_2 adsorption. In this study, CO_2 adsorption and reduction on two types of SiC nanomaterials (single layer sheet and nanotubes) are studied based on density functional theory (DFT). The theoretical investigations show that CO_2 adsorption and reduction on SiC nanomaterials display a curvature effect. SiC nanotubes with suitable curvatures can capture and reduce CO_2 effectively, while single layer SiC sheet cannot.

Computational Methods

All calculations are based on spin-polarized DFT framework as implemented in DMol^3 code.[35,36] The generalized gradient approximation (GGA) with Perdew–Burke–Ernzerhoffunctional (PBE) is employed to describe the exchange-correlation potential.[37] All electron relativistic core treatment method is implemented for relativistic effects, which explicitly includes all electrons and introduces some relativistic effects into the core. The double numerical plus

polarization (DNP) basis set is adopted for the spin-polarized DFT calculations.[35] A smearing of 0.005 Ha (1 Ha = 27.21 eV) to the orbital occupation is applied to achieve accurate electronic convergence. To ensure high-quality results, the real-space global orbital cutoff radius is chosen as high as 4.6 Å in the computations. The convergence tolerance of energy is 1.0×10^{-5} Ha, maximum force is 0.002 Ha/Å, and maximum displacement is 0.005 Å in the geometry optimization. The k-point is set as 1×1×1. The transition state (TS) for CO_2 adsorption is obtained by LST/QST tools in DMol^3 code. In order to describe the van der Waals (vdW) interaction for CO2 adsorption, the DFT + D method within Grimme scheme is adopted.[38] In calculations, the supercell models include three unit cells for (n, 0) zigzag SiC nanotubes, four unit cells for (n, n) armchair SiC nanotubes, and 5×5 supercell for single SiC layer. The minimal distance between the SiC nanotubes/sheet and their mirror images is set as 15 Å, which is sufficiently large to avoid the interaction between them. The Si-C bond length is 1.79 Å.

The adsorption energies (E_{ad}) of adsorbates on SiC are calculated through $E_{ad} = E_{ads} + E_{SiC} - E_{ads/SiC}$, where E_{ads}, E_{SiC}, and $E_{ads/SiC}$ are the total energies of an isolated adsorbate molecule, the SiC catalysts, and the adsorption systems, respectively. By these definitions, positive E_{ad} values correspond to stably exothermic adsorption processes. In order to simulate the electrochemistry environment of CO_2 electro reduction, a conductor-like screening model (COSMO) is introduced to simulate a H_2O solvent environment throughout the whole process.[39-41] Free energies of the intermediates involved in CO_2 hydrogenation are calculated based on a computational

hydrogen electrode (CHE) model suggested by Nørskov *et al*.[21,42,43] The CHE model defines that the chemical potential of a proton/electron in solution is equal to a half of the chemical potential of a gas-phase H_2. Free energy change (ΔG) of every elemental step is determined by $\Delta G = \Delta E + \Delta ZPE - T\Delta S$, where ΔE denotes the electronic energy change directly obtained from DFT calculations, ΔZPE is the change of zero point energies, T is the temperature (equals 298.15 K), and ΔS is the change in entropy. Zero point energy and entropy of the every intermediate are calculated based on the vibrational frequencies, where all the atoms are included.

Results and Discussion

The CO_2 adsorption properties of single SiC layer sheet without curvature and several SiC nanotubes with different surface curvatures are summarized in Fig. 1. Two main changes take place during the adsorption of CO_2 on SiC, i.e., the bending of the O=C=O skeleton and the binding to the surface. CO_2 prefers to be adsorbed on SiC with C-O bond attacking the Si-C bond, forming a four-membered ring. CO_2 molecule prefers to be adsorbed perpendicular to the tube axis for armchair SiC nanotubes, while it prefers to be parallel to the tube axis for zigzag SiC nanotubes (Fig. S1 of supporting information). It is found that the E_{ad} value of CO_2 on SiC nanotubes is a function of curvature. As shown in Fig. 1, the E_{ad} of CO_2 decreases gradually with decreased surface curvature of nanotube. When the diameter of the SiC nanotubes is larger than 13 Å, CO_2 molecules are physically adsorbed. This is consistent with the variation of bond lengths for Si-O and C-C bonds (Table S1 of supporting information). The bonding distances for both Si-O and C-C bonds become longer as

the diameters of SiC nanotubes increases, indicating the decrease of interactions between CO_2 and SiC nanotubes. Note that the effect of the chirality on the CO_2 adsorption is negligible as displayed in Fig. 1. For comparison, CO_2 adsorption under the consideration of vdW interaction is also calculated, as shown in Fig. 1c. Similar with previously theoretical investigation,[44] CO_2 adsorption is strengthened after considering the effect of vdW bonding. Note that the E_{ad} value of CO_2 on single layer SiC sheet is very small even after considering the vdW interaction, indicating that CO_2 cannot be adsorbed on single layer SiC sheet stably.

CO_2 adsorption and desorption under the experimental condition (at 298.15 K and 1 atm) are considered, as shown in Fig. S2 of supporting information. The activation barrier energy (E_a) of CO_2 from gas phase to adsorbed is 0.92 eV on single layer SiC sheet, which is much larger than that on (4, 4) SiC nanotube with E_a of 0.48 eV. Furthermore, the CO_2 desorption on single layer SiC sheet is much easier than that on SiC nanotubes, with E_a of 0.51 eV compared with 0.95 eV. These suggest that single layer SiC sheet cannot capture CO_2, while SiC nanotubes with suitable diameter can adsorb CO_2 stably. This is because the curvature of SiC nanotubes walls causes the electron of the SiC layers to shift from the concave inner surface to the convex outer surface resulting in CO_2 adsorption. Adsorption strength is directly proportional to curvature size. The capture capacity of CO_2 on SiC nanotubes is also examined, as shown in Table S2 and Fig. S3 of supporting information. There are 32 CO_2 molecules adsorbed on (4, 4) SiC nanotube, corresponding to a coverage of 1 monolayer (ML) (1 ML is defined as one CO_2 molecule per Si-C dimer). As the

diameter increases from 6.833 Å for (4, 4) SiC nanotube to 10.297 Å for (6, 6) SiC nanotube, the adsorption strength decreases from strong physisorption to weak physisorption and the adsorption coverage decreases to 0.5 ML on (6, 6) SiC nanotube, further testifying that the CO_2-SiC nanotube interaction becomes weaker with the increase of the tube diameter.

CO_2 hydrogenation under electrochemistry environment on single SiC layer and SiC nanotubes are studied. Producing formic acid by direct hydrogenation of CO_2 is mainly performed through a three-step process. Firstly, CO_2 is hydrogenated to a formate or a carboxyl. And then, the formate or the carboxyl is further hydrogenated to form formic acid. At last, the formic acid gets released from SiC nanotubes and sheet. As shown in Fig. 2, there exist four different routes for CO_2 hydrogenation with H^+: CO_2 can be hydrogenated either at its oxygen atom for carboxyl (COOH) formation (Paths 1 and 2), or at its carbon atom for formate (HCOO) formation with the bidentate (Path 3) or the trans (Path 4) structure adsorbed on SiC nanotubes. Taking the (4, 4) SiC nanotube as an example, the calculated free energy diagrams for the reduction of CO_2 to HCOOH at 0 V vs RHE are shown in Fig. 2. Our calculations suggest that carboxyl pathways (Paths 1 and 2) are disadvantageous compared to formate pathways (Paths 3 and 4). The ΔG values of CO_2 hydrogenation to carboxyl via Paths 1 and 2 are 1.33 and 1.57 eV, respectively, which are too large to overcome. However, the ΔG values of CO_2 hydrogenation to formate through Paths 3 and 4 are –0.19 and 0.26 eV, respectively. This is consistent with the adsorption of formate and carboxyl on (4, 4) SiC nanotube, where the adsorption of formate is stronger than

carboxyl by nearly 2 eV. Moreover, it is also found that CO_2 hydrogenation to formate intermediate is more favorable than carboxyl intermediate on Ni(111).[45] Due to the stronger adsorption of formate in bidentate structure with two O atoms binding to two Si atoms at atop sites compared with that in trans configuration with H pointing toward to the surface, the ΔG value for hydrogenation of formate with bidentate structure into formic acid (Path 3) is larger than that in trans configuration (Path 4) by 0.29 eV. In addition, desorption of formic acid in Path 4 on (4,4) SiC nanotube is easier than that in Path 3. Therefore, formate pathway with trans formate as intermediate (Path 4) is the most energy favorable one and will be further investigated for the purposes of this study.

The calculated free energy diagrams of the lowest-energy pathways for CO_2 capture and reduction on single layer SiC sheet and nanotubes are summarized in Fig. 3, shown at 0 V *vs* RHE. The overall process of CO_2 capture and reduction is almost thermodynamically neutral. As the curvature of SiC nanotubes decreases, the ΔG values for CO_2 reduction decrease. The energy needed for the whole reduction process of CO_2 on (2,2) SiC nanotube are 7 times higher compared with (8,8) SiC nanotube. CO_2 capture and reduction on single layer SiC sheet and nanotubes follow the Sabatier principle.[46,47] The interactions between reactants and catalysts cannot be too strong or too weak.[48-50] For SiC nanotubes (diameters smaller than 6 Å) that bind CO_2 too strongly, the rate of CO_2 reduction is limited by the removal of adsorbed reduction intermediates. For SiC nanotubes (diameters larger than 13 Å) and single layer SiC sheet that bind CO_2 too weakly, the rate is limited by the activation of CO_2, or more

likely, the transfer of electrons and protons to adsorbed CO_2. As seen in Fig. 3, SiC nanotubes with diameters of 7~12 Å bind CO_2 intermediately as compared to other SiC nanotubes and single layer sheets. At (2,2) armchair SiC nanotube, the ΔG for CO_2 adsorption is as large as –1.83 eV and the ΔG values for the three steps of the CO_2 reduction are 0.60, 0.60 and 0.61 eV, respectively. At (6,6) armchair SiC nanotube, the ΔG for CO_2 adsorption increases to –0.47 eV, and the E_r values for the three steps of CO_2 reduction decrease to 0.15, 0.10 and 0.26 eV, respectively, which are much smaller than that on CODH and similar to that on tin oxide nanoparticles,[25,51] suggesting high activities of CO_2 reduction. Upon further increasing the diameter of SiC nanotubes to 13 Å, although the ΔG value for CO_2 reduction is very small, SiC nanotubes cannot capture CO_2 efficiently due to the weak adsorption.

Similar with CO_2 adsorption, the effect of chirality on CO_2 reduction is also very small, as shown in Fig. 3. Such a remarkable agreement can be attributed to the localized characteristics of the CO_2-SiC interaction. This is consistent with the interaction between CO_2 and boron-rich BN nanotubes, which also shows localized characteristics.[17]

In order to gain further insight into the origin of the interaction between CO_2 and SiC, the electronic structures of the above materials are studied. Fig. 4 illustrates the spin-polarized partial density of states (PDOS) projected onto the CO_2 and SiC. In free CO_2 molecule, the highest occupied molecular orbital (HOMO) is the $1\pi_g$ orbital, while the lowest unoccupied molecular orbital (LUMO) is the $2\pi_u$ orbital. When the

O=C=O skeleton was bent, the LUMO of $2\pi_u$ split into $6a_1$ and $2b_1$.[52-54] As a consequence, the $6a_1$ orbital becomes the LUMO. The resulting LUMO orbital shows σ-orbital and π-orbital characteristics, and can interact effectively with the *p*-orbitals for charge transfer from SiC to CO_2. Since the C-O orbital in $6a_1$ has an anti-bonding characteristic, the stronger the electron transfer, the stronger the anti-bonding and therefore the longer the C-O bond is. The renowned electron donation-back-donation mechanism contributes to the interaction between the CO_2 and SiC.[17] During the adsorption process of CO_2 on the surface, electrons are transferred from Si-2*p* states to CO_2-$6a_1$ orbital and are back donated from CO_2-$1\pi_g$ orbital to C-2*p* states, which result in the shift of CO_2-$6a_1$ to lower energies below the Fermi level E_f and the degeneration of CO_2-$1\pi_g$, as shown in Fig. 4. The electron transfer to the anti-bonding LUMO orbital weakens the C=O bonds in the adsorbed molecule. To mix with surface Si-2*p* and C-2*p* orbitals, the 2*p* states of the adsorbed CO_2 broaden, compared to those of a free CO_2. This signature is common for molecules interacting with solid surfaces as predicted by the Newns-Anderson model.[55] From electron density difference (Fig. S4 in supporting information), one can therefore conclude that there must be a fairly substantial covalent contribution to the C-C bond and ionic contribution to the Si-O bond between CO_2 and SiC. As shown in Tables S3 and S4 of supporting information, when the curvature of the SiC nanotubes decreases, the positive charge of the Si atoms increases while the charge transfer from Si atom to O-CO_2 atom and from C-CO_2 to C atom of SiC decrease, resulting in weaker interactions between SiC and CO_2.

Conclusions

In conclusion, theoretical DFT calculations were performed on single layer SiC sheet and nanotubes to ascertain the catalytic activity toward CO_2 adsorption and reduction. It is found that CO_2 adsorption and reduction significantly depend on the surface curvature of SiC nanomaterials. CO_2 cannot be adsorbed on single layer SiC sheet, while SiC nanotubes with diameter smaller than 13 Å can catch it stably. As the curvature of SiC nanotubes decreases, both the adsorption energy and reduction free energy values of CO_2 decrease. These findings give insight into the unique structure-property relationship following Sabatier principle, which are particularly valuable for the design and development of new materials that would generate fuels with a carbon-neutral footprint using aqueous solutions of electrocatalysts for CO_2 reduction at low over-potentials.

Acknowledgments

The authors acknowledge financial support from the National Natural Science Foundation of China (No. 21403092), the Natural Science Foundation of Jiangsu (No. BK20130519), the China Postdoctoral Science Foundation (No. 2013M541611 and 2014M550270), the Senior Intellectuals Fund of Jiangsu University (No. 12JDG094 and 13JDG032) and the Danish National Research Foundation and the Danish Ministry of Science, Technology, and Innovation through Center for DNA Nanotechnology (CDNA), interdisciplinary Nanoscience Center (iNANO) and the Danish Research Councils.

Reference

1 T. R. Karl and K. E. Trenberth, *Science*, 2003, **302**, 1719-1723.

2 D. W. Keith, *Science*, 2009, **325**, 1654-1655.

3 R. S. Haszeldine, *Science*, 2009, **325**, 1647-1652.

4 Z. L. Wang, J. M. Yan, H. L. Wang, Y. Ping and Q. Jiang, *Sci. Rep.*, 2012, **2**, 598.

5 Z. L. Wang, J. M. Yan, Y. Ping, H. L. Wang, W. T. Zheng and Q. Jiang, *Angew. Chem. Int. Ed.*, 2013, **52**, 4406-4409.

6 B. Wang, A. P. Cote, H. Furukawa, M. O'Keeffe and O. M. Yaghi, *Nature*, 2008, **453**, 207-211.

7 O. K. Farha, A. Özgür Yazaydın, I. Eryazici, C. D. Malliakas, B. G. Hauser, M. G. Kanatzidis, S. T. Nguyen, R. Q. Snurr and J. T. Hupp, *Nat. Chem.*, 2010, **2**, 944-948.

8 Y. Xie, T. T. Wang, X. H. Liu, K. Zou and W. Q. Deng, *Nat. Commun.*, 2013, **4**, 1960.

9 H. A. Patel, S. H. Je, J. Park, D. P. Chen, Y. Jung, C. T. Yavuz and A. Coskun, *Nat. Commun.*, 2013, **4**, 1357.

10 A. B. Vidal, L. Feria, J. Evans, Y. Takahashi, P. Liu, K. Nakamura, F. Illas and J. A. Rodriguez, *J. Phys. Chem. Lett.*, 2012, **3**, 2275-2280.

11 J. Wei, D. Zhou, Z. Sun, Y. Deng, Y. Xia and D. A. Zhao, *Adv. Funct. Mater.*, 2013, **23**, 2322-2328.

12 J. Park, H. Kim; S. S. Han and Y. Jung, *J. Phys. Chem. Lett.*, 2012, **3**, 826-829.

13 D. Feng, W. C. Chung, Z. Wei, Z. Y. Gu, H. L. Jiang, Y. P. Chen, D. J. Darensbourg and H. C. Zhou, *J. Am. Chem. Soc.*, 2013, **135**, 17105-17110.

14 M. M. Deshmukh, M. Ohba, S. Kitagawa and S. Sakaki, *J. Am. Chem. Soc.*, 2013, **135**, 4840-4849.

15 D. Liu, J. Gu, Q. Liu, Y. Tan, Z. Li, W. Zhang, Y. Su, W. Li, A. Cui, C. Gu and D. Zhang, *Adv. Mater.*, 2014, **26**, 1229-1234.

16 D. S. Zhang, Z. Chang, Y. F. Li, Z. Y. Jiang, Z. H. Xuan, Y. H. Zhang, J. R. Li, Q. Chen, T. L. Hu and X. H. Bu, *Sci. Rep.*, 2013, **3**, 3312.

17 H. Choi, Y. C. Park, Y. H. Kim and Y. S. Lee, *J. Am. Chem. Soc.*, 2011, **133**, 2084-2087.

18 Q. Sun, Z. Li, D. J. Searles, Y. Chen, G. M. Lu and A. Du, *J. Am. Chem. Soc.*, 2013, **135**, 8246-8253.

19 Y. Yang, M. G. White and P. Liu, *J Phys. Chem. C*, 2012, **116**, 248-256.

20 K. Sekizawa, K. Maeda, K. Domen, K. Koike and O. Ishitani, *J. Am. Chem. Soc.*, 2013, **135**, 4596-4599.

21 A. A. Peterson, F. Abild-Pedersen, F. Studt, J. Rossmeisl and J. K. Nørskov, *Energy Environ. Sci.*, 2010, **3**, 1311-1315.

22 X. Nie, M. R. Esopi, M. J. Janik and A. Asthagiri, *Angew. Chem. Int. Ed.*, 2013, **52**, 2459-2462.

23 J. H. Kwak, L. Kovarik and J. Szanyi, *ACS Catal.*, 2013, **3**, 2449-2455.

24 K. P. Kuhl, E. R. Cave, D. N. Abram and T. F. Jaramillo, *Energy Environ. Sci.*, 2012, **5**, 7050-7059.

25 J. B. Varley, H. A. Hansen, N. L. Ammitzbøll, L. C. Grabow, A. A. Peterson, J. Rossmeisl and J. K. Nørskov, *ACS Catal.*, 2013, **3**, 2640-2643.

26 D. J. Boston, C. Xu, D. W. Armstrong and F. M. Macdonnell, *J. Am. Chem. Soc.*, 2013, **135**, 16252-16255.

27 C. A. Huff and M. S. Sanford, *ACS Catal.*, 2013, **3**, 2412-2416.

28 A. Karelovic and P. Ruiz, *ACS Catal.*, 2013, 3, 2799-2812.

29 A. S. Varela, C. Schlaup, Z. P. Jovanov, P. Malacrida, S. Horch, I. E. L. Stephens and I. Chorkendorff, *J. Phys. Chem. C*, 2013, **117**, 20500-20508.

30 J. Ye, C. Liu, D. Mei and Q. Ge, *ACS Catal.*, 2013, **3**, 1296-1306.

31 H. A. Hansen, J. B. Varley, A. A. Peterson and J. K. Nørskov, *J. Phys. Chem. Lett.*, 2013, **4**, 388-392.

32 A. A. Peterson and J. K. Nørskov, *J. Phys. Chem. Lett.*, 2012, **3**, 251-258.

33 M. Z. Ertem, S. J. Konezny, C. M. Araujo and V. S. Batista, *J. Phys. Chem. Lett.*, 2013, **4**, 745-748.

34 E. B. Cole, P. S. Lakkaraju, D. M. Rampulla, A. J. Morris, E. Abelev and A. B. Bocarsly, *J. Am. Chem. Soc.*, 2010, **132**, 11539−11551.

35 B. Delley, *J. Chem. Phys.*, 1990, **92**, 508-517.

36 B. Delley, *J. Chem. Phys.*, 2000, **113**, 7756-7764.

37 J. P. Perdew, K. Burke and M. Ernzerhof, *Phys. Rev. Lett.*, 1996, **77**, 3865-3868.

38 S. Grimme, *J. Comput. Chem.*, 2006, **27**, 1787-1799.

39 A. Klamt and G. Schuurmann, *J. Chem. Soc. Perkin Trans.*, 1993, **2**, 799-805.

40 B. Delley, *Mol. Simul.*, 2006, **32**, 117-123.

41 J. Andzelm, C. Kölmel, and A. Klamt, *J. Chem. Phys.*, 1995, **103**, 9312-9320.

42 J. K. Nørskov, J. Rossmeisl, A. Logadottir, L. Lindqvist, J. R. Kitchin, T. Bligaard

and H. Jónsson, *J. Phys. Chem. B*, 2004, **108**, 17886-17892.

43 L. Yu, X. Pan, X. Cao, P. Hu, X. Bao, *J. Catal.*, 2011, **282**, 183-190.

44 P. Zhang, B. B. Xiao, X. L. Hou, Y. F. Zhu and Q. Jiang, *Sci. Rep.*, 2014, **4**, 3821.

45 G. Peng, S. J. Sibener, G. C. Schatz, S. T. Ceyer and M. Mavrikakis, *J. Phys. Chem. C*, 2012, **116**, 3001-3006.

46 Q. T. Trinh, J. Yang, J. Y. Lee and M. Saeys, *J. Catal.*, 2012, **291**, 26-35.

47 J. L. Lin and I. Wheeldon, *ACS Catal.*, 2013, **3**, 560-564.

48 V. Stamenkovic, B. S. Mun, K. J. J. Mayrhofer, P. N. Ross, N. M. Markovic, J. Rossmeisl, J. Greeley and J. K. Nørskov, *Angew. Chem. Int. Ed.*, 2006, **45**, 2897-2901.

49 J. Greeley, I. E. L. Stephens, A. S. Bondarenko, T. P. Johansson, H. A. Hansen, T. F. Jaramillo, J. Rossmeisl, I. Chorkendorff and J. K. Nørskov, *Nat. Chem.*, 2009, **1**, 552-556.

50 J. K. Nørskov, T. Bligaard, J. Rossmeisl and C. H. Christensen, *Nat. Chem.*, 2009, **1**, 37-46.

51 S. Zhang, P. Kang and T. J. Meyer, *J. Am. Chem. Soc.*, 2014, **136**, 1734-1737.

52 Q. L. Tang and Q. H. Luo, *J. Phys. Chem. C*, 2013, **117**, 22954-22966.

53 S. G. Wang, X. Y. Liao, D. B. Cao, C. F. Huo, Y. W. Li, J. Wang and H. Jiao, *J. Phys. Chem. C*, 2007, **111**, 16934-16940.

54 C. Cazorla, S. A. Shevlin and Z. X. Guo, *J. Phys. Chem. C*, **2011**, *115*, 10990-10995.

55 D. M. Newns, *Phys. Rev.*, 1969, **178**, 1123-1135.

Captions:

Fig. 1. (a) Schematic profile of CO_2 adsorbed on single SiC layer and SiC nanotubes. Gray, gold and red colors denote C, Si and O atoms, respectively. Adsorption energies of CO_2 on single layer SiC sheet and nanotubes without (b) and with (c) the consideration of van der Waals interaction.

Fig. 2. (a-d) Free energy diagrams of four pathways for CO_2 hydrogenation on (4, 4) SiC nanotube. Gray, gold and red colors denote C, Si and O atoms, respectively.

Fig. 3. Free energy diagrams of CO_2 hydrogenation on single SiC layer and armchair (a) and zigzag (b) SiC nanotubes.

Fig. 4. Partial density of states (PDOS) for CO_2 adsorbed on (4, 4) armchair SiC nanotubes.

Fig. 1.

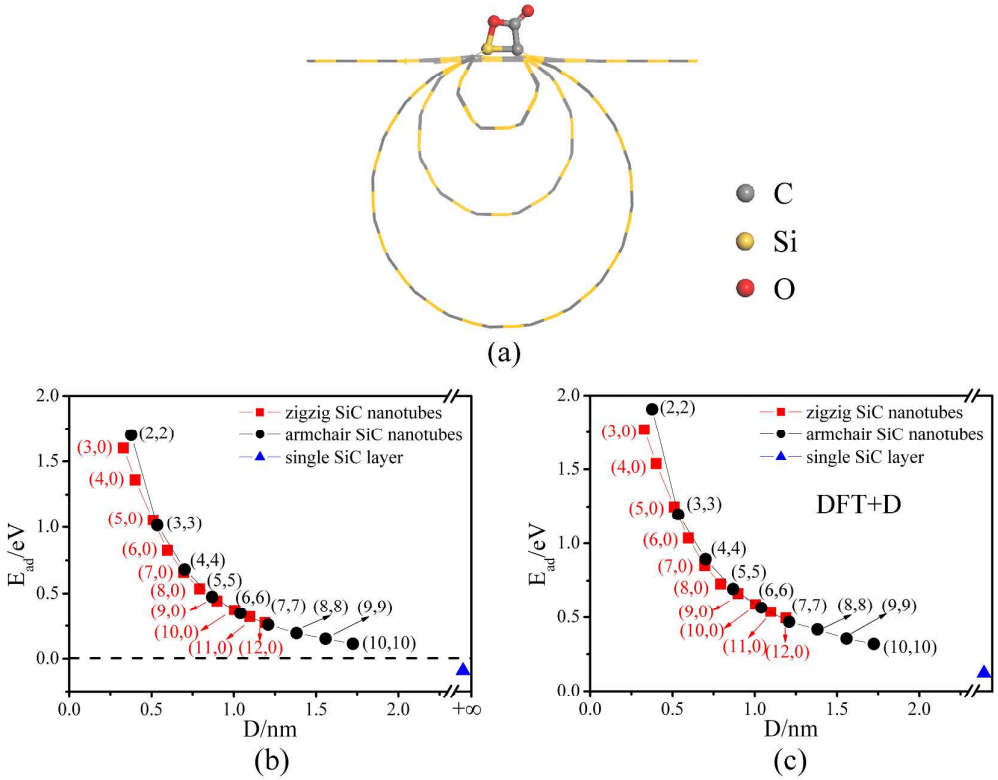

Fig. 2.

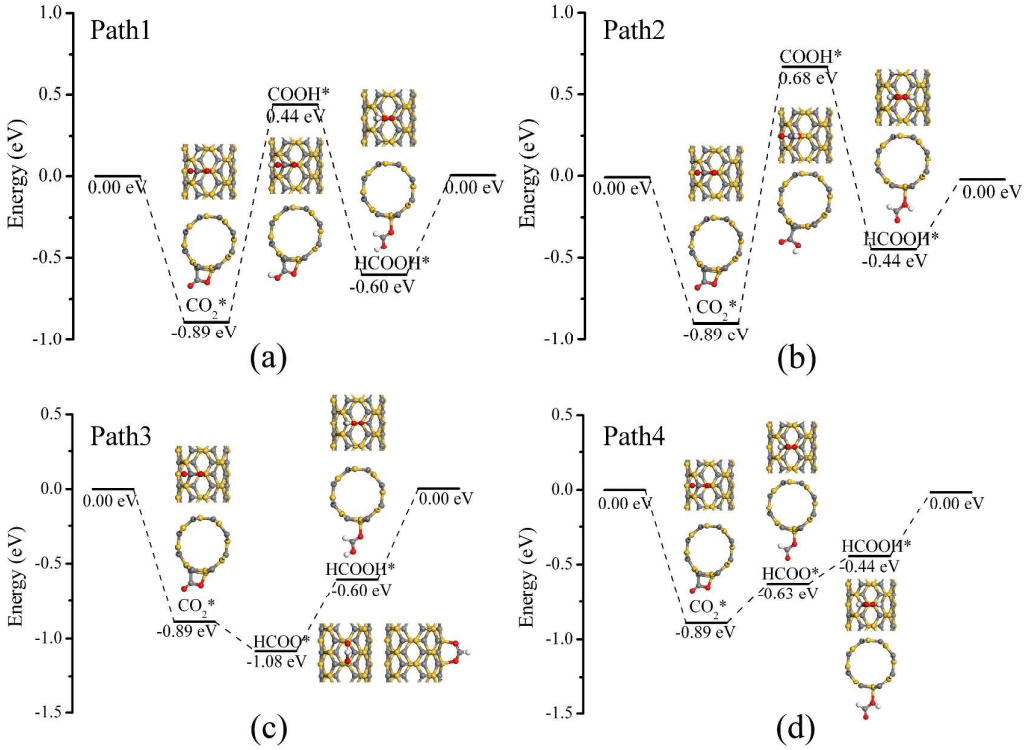

Fig. 3.

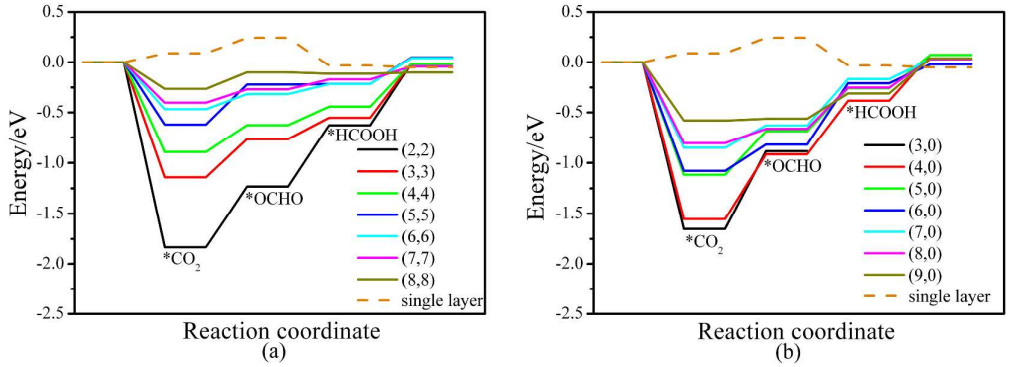

Fig. 4.